DOI: https://doi.org/10.68732/a104fd6b83495b5c

ISBN: 978-9989-2053-6-1

Microstructural analysis of granite tested under uniaxial compression

L. C. Witte, M. Duda, A. Chehreh, S. C. Pansa, T. Backers
Ruhr University Bochum, Bochum, Germany
Lucas.witte@ruhr-uni-bochum.de

Abstract

Detailed knowledge of the microstructural damage before, during and after loading is needed for a better understanding of the mechanisms leading to macroscopic failure of crystalline rocks. This is particularly true for granite, which is being discussed (Germany) or has already been selected (Finland, Sweden) as a potential host rock for radioactive waste disposal. Therefore, it is important to evaluate the long-term stability and integrity of such subsurface storage systems in granite. This study examined the microstructure of uniaxially loaded granite up to 40 %, 60 %, 80 %, and almost to and beyond its uniaxial compressive strength. Deformed granite specimens were saturated in coloured epoxy resin before thin sections were prepared from central parts of the cylindrical specimens. The results indicate an increase in number of cracks with increasing maximum axial stress. The resulting crack pattern shows main fractures and fine inter- and intragranular cracks. Both, tensile and shear cracks were identified, while cracks oriented subparallel to the axial stress direction were dominant in most thin sections. Finely ground mineral grains occur in areas of significant damage. These results provide valuable insights into the micromechanical processes of crack initiation and propagation in uniaxially loaded granitic rock samples. They improve the understanding of the mechanical stability of a potential host rock and serve as a basis for further numerical simulations to describe and predict failure mechanisms.

Keywords

Microstructure, Crack analysis, Uniaxial compressive strength, Granite, Nuclear waste disposal.

1 Introduction

The mechanical behaviour of rocks under compressive stress is significantly controlled by the initiation, growth and interaction of microcracks (Brace et al. 1966; Bieniawski 1967). While parameters such as uniaxial compressive strength (UCS) and Young´s modulus are determined according to standards (ISRM 1979; DGGT 2022), the visual correlation between internal damage development and macroscopic failure behaviour is less frequently analysed. While Kranz (1983) discussed the type and distribution of cracks in different rocks, Scholz (1968), Lockner (1993), Heap et al. (2009) and many others investigated the temporal development of microcracks using acoustic emission detection.

The present study provides a detailed examination of crack development in crystalline rock, with a particular focus on the quantitative analysis of microcrack kinetics at different stress levels. Using a combination of mechanical laboratory tests and high-resolution, digitally supported thin section

analysis, the study examines how crack density, orientation and distribution patterns change as a function of axial load. The aim is to get a better understanding of the micromechanical processes leading to the transition from micro- to macroscopic failure.

2 Material and methods

2.1 Sample material

Uniaxial compressive strength tests were carried out on a dense, highly granular granite originating from Padang, China. Its medium-sized grains exhibit very high grain bond strength and appear macroscopically isotropic. The mineralogical composition, derived from X-ray powder diffraction analysis, is dominated by plagioclase, quartz, and feldspar (Fig. 1), which account for 40 ± 5 vol.%, 32 ± 3 vol.%, and 23 ± 3 vol.%, respectively. Minor constituents include biotite with 4 ± 2 vol.% and muscovite/illite with less than 1 vol.%.

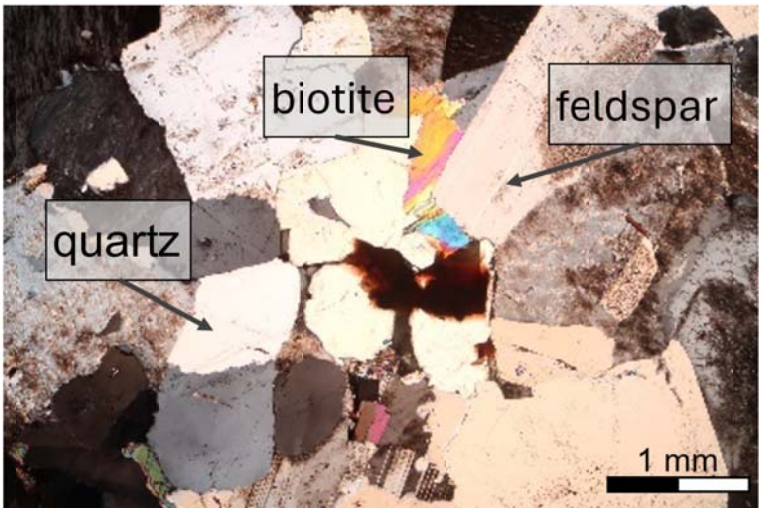


Fig. 1 Optical image in cross-polarized light for thin section orientation of Padang Granite Block 2 in X-Z plane.

2.2 Methods

2.2.1 Uniaxial compressive strength tests

Specimens of 40 mm diameter and 80 mm length were prepared and tested in accordance with DGGT (2022) and ISRM (1979). The specimens were placed in a stiff 4 MN loading frame and centred between a lower and upper spherical seated loading platen. Experiments were performed using graphite powder as lubricant between loading piston and specimen´s end faces to reduce friction. A radial strain chain was placed at the centre of the specimen. Tests were conducted servo-controlled with grade one testing equipment. During testing, axial load was applied to approximately 40 %, 60 %, 80 % of the previously determined reference UCS of 225 MPa. Two further experiments were terminated at maximum strength and after macroscopic failure. Young´s modulus E and Poisson´s ratio υ were determined between 30 % and 40 % of the hypothetical UCS of 225 MPa using axial strains that were calibrated for system characteristics.

2.2.2 Thin section preparation and microstructural analysis

An undeformed reference specimen and uniaxially tested pre- and post-failure granite specimens were saturated in blue epoxy resin after vacuum treatment to preserve microfracture characteristics of the specimen volume (Table 1). The specimen was subsequently cut perpendicular to the main fracture, if visible, and parallel to the axial stress direction. Thin-sections of approximately 30 µm thickness were prepared. In total, 14 thin-sections from seven specimens were investigated.

Thin-section images were recorded with a digital microscope. Images were captured at a magnification of 100 in grid-based mode using a motorised object table and automatically combined to an image showing the complete thin section. A ring light was used for illumination. The brightness was automatically controlled to ensure optimal exposure conditions. To compensate for potential unevenness of the thin section's surface and to ensure a consistently sharp image, automatic height compensation was used in the z-axis. Maximum image sizes of up to 20.000 × 20.000 pixels (≈ 2 µm/px) were achieved, enabling a high-resolution and comprehensive visualisation of the microstructural characteristics.

The microstructure was analysed manually by visually scanning full thin section images. Each microcrack was digitised by two endpoints, converted from pixel-to-µm coordinates using the image scale, and idealised as a straight line. Only epoxy filled cracks were identified, assuming they were coalescing to form the main fracture eventually leading to macroscopic failure, and to avoid confusion with cleavage planes or grain boundaries. Individual tensile and shear cracks were distinguished, primarily based on abrupt orientation changes not attributable to stiffness contrasts. The main fracture was excluded, as the focus is on crack kinetics leading to macroscopic failure through crack coalescence. Dense crack networks were omitted due to identification uncertainty. In complex systems, crack patterns were assessed on a case-by-case study.
Crack statistics were evaluated individually for each specimen using the equations summarised in Table 2. For each specimen, crack datasets from the two separate thin sections were combined. The total number of cracks was counted. Crack length and orientation were calculated from digitised crack endpoints. Mean crack length, crack density, and crack intensity were determined. Crack length histograms were created using 5 µm (reference specimen) or 50 µm (all other specimens) intervals. The most common crack length was estimated by fitting a log-normal distribution. Polar histograms of crack orientations were analysed in 10° intervals. Tensile and shear cracks were evaluated separately. Cracks with an inclination angle of ≤17° to the axial stress direction were classified as tensile cracks, all others as shear cracks. Crack density and intensity maps were derived on a 1 mm × 1 mm grid using crack centre positions.

Table 1. Thin-section photos of specimens deformed uniaxially at 10^{-5} s^{-1} and stopped at different deformation stages.

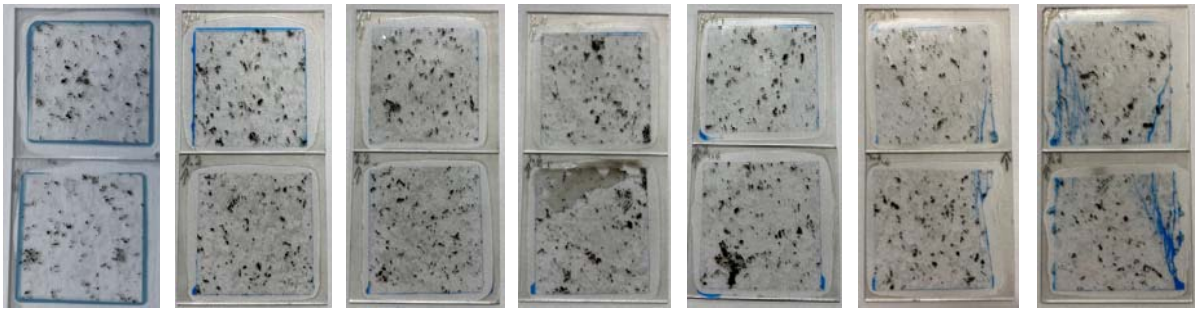
Reference and dry specimens deformed at 10-5 s-1 up to given stages during UCS						
UP0 Reference	UP1-40 40 %	UP2-60 60 %	UP3-80 80 %	UP4-BF Before failure	UP5-AF At failure	UP6 Beyond failure
						

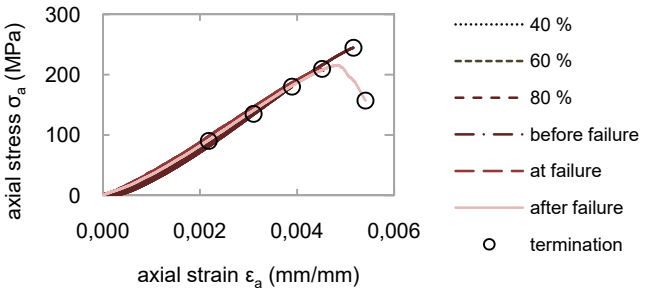
Table 2. Calculation of crack geometry parameters in individual specimens. Individual crack coordinates are represented by their endpoints through $x_{1,i}$, $y_{1,i}$ and $x_{2,i}$, $y_{2,i}$. *Analog calculation for tensile and shear cracks.

parameter	**description**	**calculation**
x_{mode}	Mode of log-normal distribution (PDF) based on its mean $\mu_{\ln}$ and standard deviation $\sigma_{\ln}$	$x_{\mathrm{mode}} = e^{\mu_{\ln} - {\sigma_{\ln}}^2}$
A_{c}	Area covered by cracks	$A_{\mathrm{c}} = [\max(x_i) - \min(x_i)] \cdot [\max(y_i) - \min(y_i)]$
ρ_{c}	Crack density	$\rho_{\mathrm{c}} = \frac{n_{\max}}{A_{\mathrm{c}}}$
I_{c}	Crack intensity	$I_{\mathrm{c}} = \frac{\sum_i^{n_{\max}} L_{c,i}}{A_{\mathrm{c}}}$

3 Results

3.1 Uniaxial compressive strength tests

Young's moduli and Poisson's ratios vary between 51.7 and 54.5 GPa, and 0.18 and 0.35, respectively (Fig. 2). The stress-strain relations show a similar pattern up to the respective stress levels. At the beginning, a slightly curved phase indicates the closure of pre-existing microcracks. With increasing axial strain, the behaviour transitions to a linear section describing a nominally elastic deformation. Shortly before failure, a deviation from linear behaviour can be observed, which is associated with the initiation and growth of new microcracks. Reaching the maximum stress is followed by a significant stress drop, which marks the brittle macroscopic failure of the specimen.



specimen	σ_{max} (MPa)	E (GPa)	υ (-)
UP1-40 %	90.2	54.5	0.21
UP2-60 %	135.1	54.1	0.24
UP3-80 %	180.2	54.5	0.18
UP4-BF	244.7	52.5	0.35
UP5-AF	209.5	52.0	0.22
UP6-afterF	215.6	51.7	0.18

Fig. 2 Results of UCS tests. Left: Stress-strain relations of uniaxial deformation until termination. Right: Maximum axial stress σ_{max}, Youngs´s modulus E, and Poission´s ratioυ of specimens loaded to 40 %, 60 %, 80 % of UCS, immediately before (BF), at (AF) and after failure (after F).

3.2 Microstructural analysis

In the reference specimen, 93 cracks were identified, most of which exhibit a sub-horizontal orientation. Crack lengths vary between 13 µm and 541 µm, with the maximum frequency occurring in the interval from 55 µm to 60 µm (Fig. 3). The mode representing the most frequent crack length after fitting a log-normal distribution is 48 µm. The total number of cracks increases with increasing axial stress (Fig. 4). A significant increase can be seen as the granite approaches its UCS. This applies to both tensile and shear cracks. The ratio of number of tensile to number of shear cracks increases from 0.15 to 1.04 (Fig. 4 b). At 40 % of the UCS, the orientation of the cracks is still largely similar to that of the reference specimen. With increasing maximum axial stress, tensile cracks increasingly dominate (Fig. 4Fig. 5).

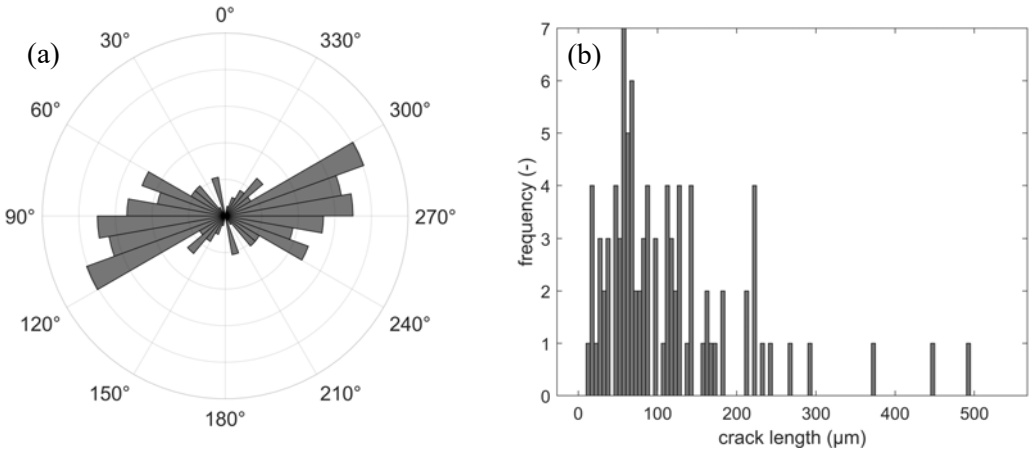


Fig. 3 (a) Frequency distribution of crack orientations in thin section of the Padang granite reference specimen. Radial axes are normalised to total crack number and radial scale ranges from 0 to 0.1. (b) Frequency (number of cracks) distribution of crack lengths (tensile and shear) in intervals of 5 µm.

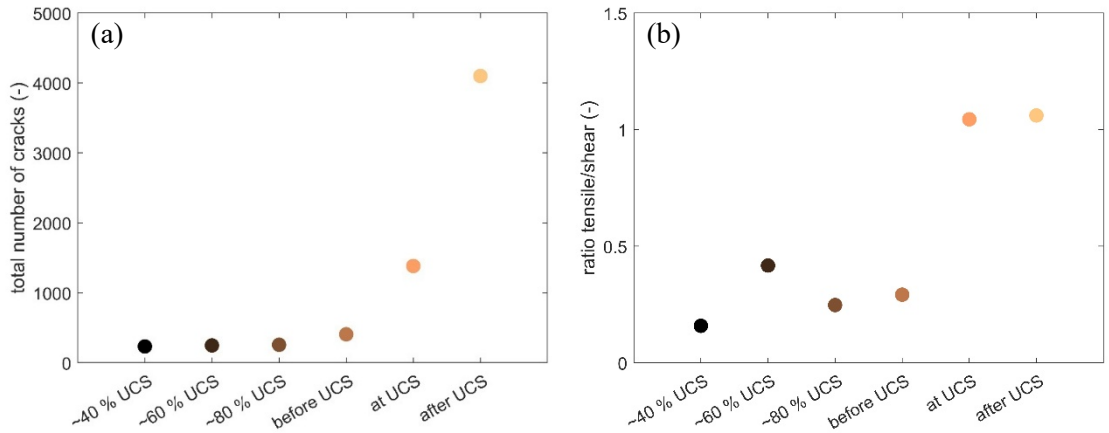


Fig. 4(a) Total number of cracks and (b) ratio of number of tensile to shear cracks in thin sections of Padang granite specimens uniaxially deformed up to different stages.

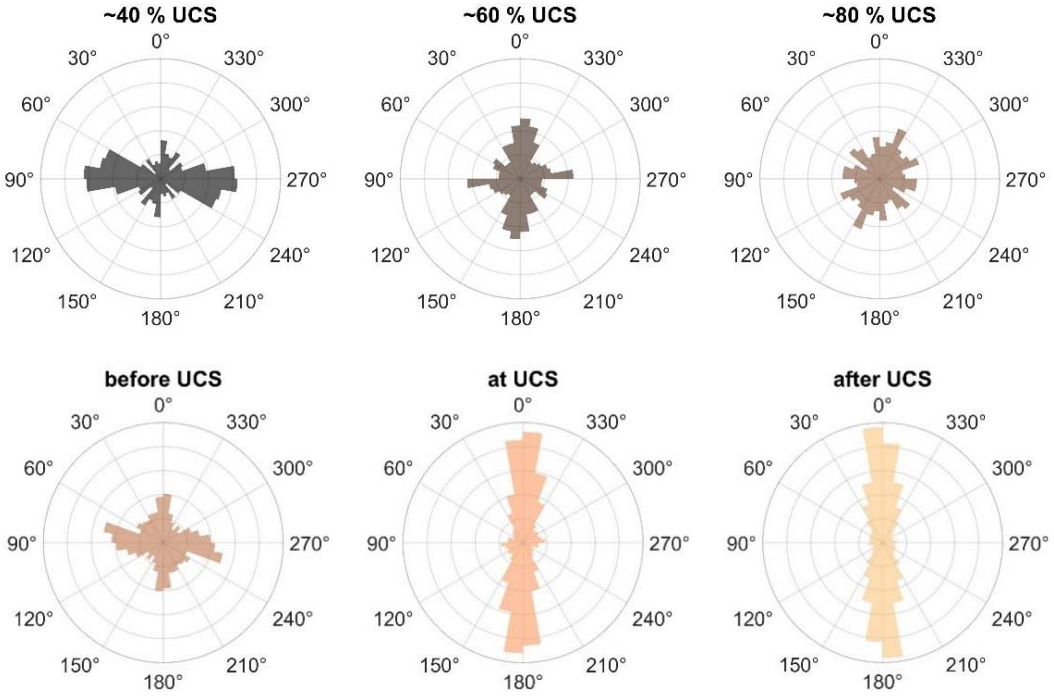


Fig. 5 Frequency distribution of crack orientations in thin sections of Padang granite specimens uniaxially deformed up to different stages. Radial axes are normalised to total crack number in each specimen and radial scale ranges from 0 to 0.1.

Histograms of crack length distributions show a log-normal distribution for all specimens, an increase in the total number of cracks across most length intervals and an increase in maximum crack lengths from 2.0 mm to 5.8 mm (Fig. 6). The mode (most frequent crack length) shows an initial increase with increasing axial stress, which, however, is predominantly attributable to the first 60 % of the axial stress and already approximately twice as large as in the reference specimen at 40 % of the UCS (Fig. 7a). Crack density and crack intensity also increase, in accordance with the increasing number of cracks (Fig. 7b, c).

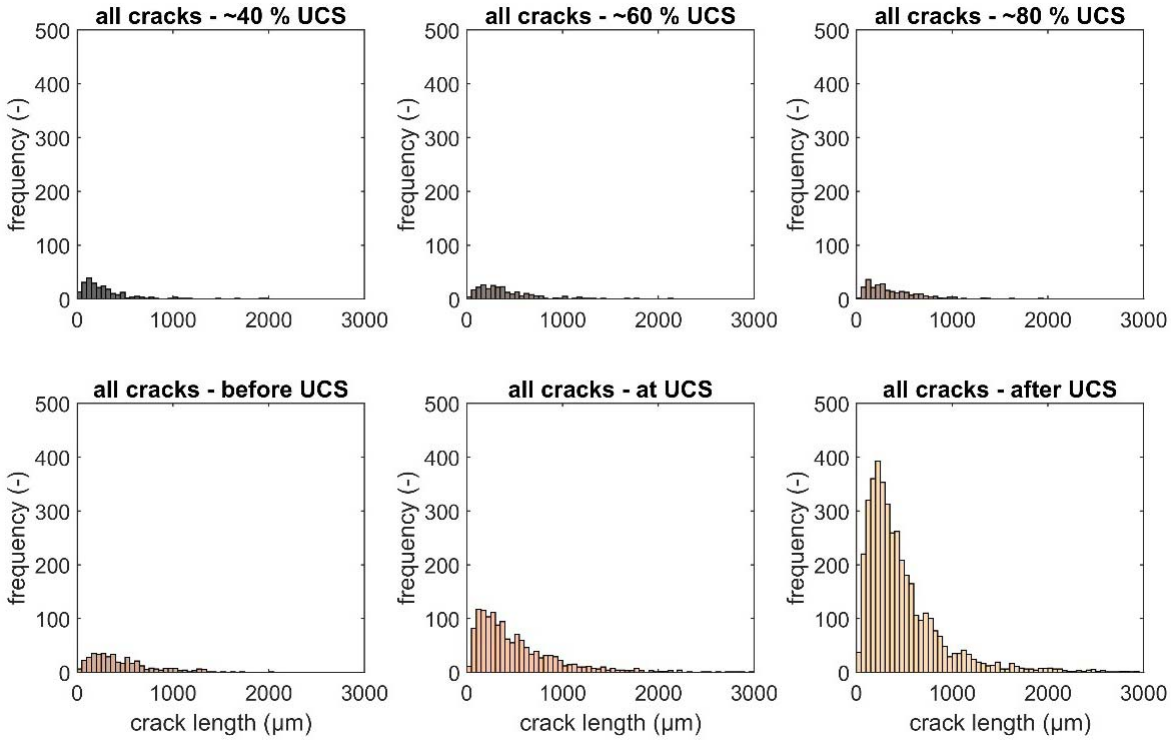


Fig. 6 Frequency distribution of crack lengths (tensile and shear) in intervals of 50 µm in thin sections of Padang granite specimens uniaxially deformed up to different stages.

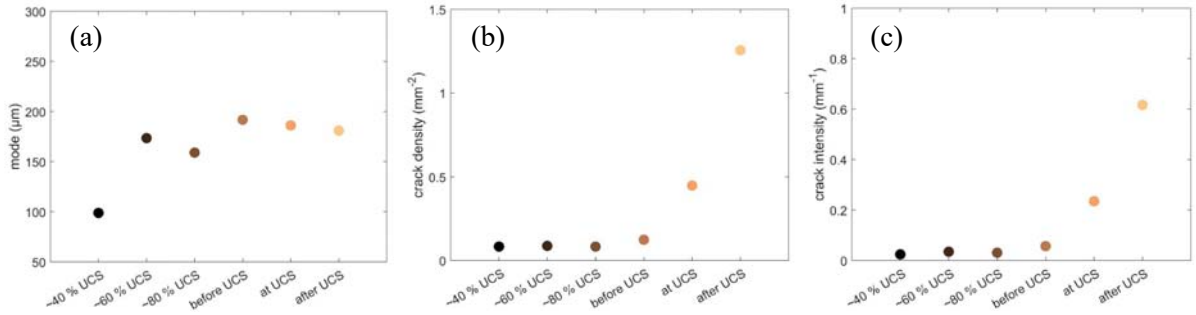


Fig. 7 Mode of log-normal crack length distribution, crack density, and crack intensity in thin sections of Padang granite specimens uniaxially deformed up to different stages.

4 Discussion

The crack inventory of the investigated granite specimens shows a clear correlation between applied maximum axial stress and development of microcracks. As stress increases, the number, density and intensity of the cracks increase. The development in modal crack length with increasing stress indicates that damage is controlled by the growth and coalescence of microcracks. The subsequent flattening of the mode shows that, regardless of a further increase in stress, the dominant microcrack length remains constant, pointing to crack interaction at stresses as low as 60 % of UCS rather than further growth leading to macroscopic failure. For the systematic recording of the crack systems, only cracks filled with blue-coloured epoxy resin were considered and digitised manually using complete thin section images allowing to create a consistent and statistically reliable data basis. To minimise interpretation bias, all cracks were identified by a single person and analysed only after the entire data set had been recorded. The data set clearly shows the relationship between stress and microstructural crack development and offers potential for the calibration of numerical models.

5 Conclusion

This study presents a quantitative microstructural analysis of thin sections prepared from uniaxially tested granite specimens that were subjected to different stress levels. Crack properties were systematically related to increasing maximum axial stress. Total number, length, density and intensity of cracks increased with increasing stress, and a transition from shear- to tensile-dominated crack inventory was observed towards failure. Tensile cracks control the macroscopic failure of granite in uniaxial experiments, whilst dominant crack length does not change significantly beyond 60 % of UCS. A thorough microstructural analysis of the crack inventory is a direct and promising approach to quantify and better understand the mechanisms leading to macroscopic failure.

Aspects of this work were performed within the projects BeNuQuA and MicroBeNuQuA (funded by the Swedish Radiation Safety Authority SSM, Sweden), and AGENS (funded by the German FederalMinistry for Economic Affairs and Energy). We acknowledge the support for our research.

References

Bieniawski, Z. T. (1967). Mechanism of brittle fracture of rock. International Journal of Rock Mechanics and Mining Sciences, 4(4), 395–430. DOI. 10.1016/0148-9062(67)90030-4

Brace, W. F., Paulding, B. W. & Scholz, C. H. (1966). Dilatancy in the fracture of crystalline rocks. Journal of Geophysical Research, 71(16), 3939–3953. DOI. 10.1029/JZ071i016p03939

Heap, M. J., Baud, P., Meredith, P. G., Vinciguerra, S. & Bell, A. F. (2009). Time-dependent brittle deformation of sandstone. Journal of Geophysical Research, 114, B07202. DOI. 10.1029/2008JB006042

Kranz, R. L. (1983). Microcracks in rocks: A review. Tectonophysics, 100(1–3), 449–480. DOI. 10.1016/0040-1951(83)90198-1

Lockner, D. A. (1993). The role of acoustic emission in the study of rock fracture. International Journal of Rock Mechanics and Mining Sciences, 30(7), 883–899. DOI. 10.1016/0148-9062(93)90041-B

Scholz, C. H. (1968). Microfracturing and the inelastic deformation of rock in compression. Journal of Geophysical Research, 73(4), 1417–1432. DOI. 10.1029/JB073i004p01417